Supporting Information

Magnetism in a Helicate Complexes Arising with the Tetradentate Ligand

Hitomi Ohmagari, Manabu Nakaya, Kaisei Tanaka, Hikaru Zenno, Ryohei Akiyoshi, Yoshihiro Sekine, Yingjie Zhang, Kil Sik Min, Miki Hasegawa, Leonard F. Lindoy, and Shinya Hayami

Synthesis

Dimphen (1,2-Bis(9-methyl-1,10-phenanthrolin-2-yl) ethane) were prepared by the synthetic route depicted in Scheme S1. Metal complexes ([Fe(dimphen)$(NCS)_2$] (**1**), [Co(dimphen)$(NCS)_2$] (**2**) [Mn(dimphen)$(NCS)_2$] (**3**) and [Fe(dimphen)$(NCSe)_2$] (**4**)) are synthesized in MeOH solution and these single crystals were obtained by using H-tube glassware.

Materials.

All reagents were commercially available. THF solvent was used after distillation. Neocuproine monohydrate was co-evaporated with hexane to yield the anhydrous product.

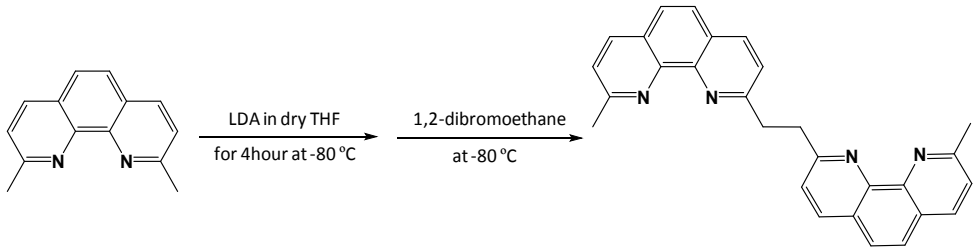

Scheme S1. Synthetic scheme of dimphen ligand.

Synthesis of dimphen[1,2]

Anhydrous Neocuproine (3.0 g, 14.4 mmol) was dissolved in distilled THF (100 mL) to a 300 mL round bottom flask. Lithium diisopropylamide (28.8 mmol) was added dropwise via a cannula at –80°C. The final deep colors for monocarbanion was black-brown. After stirring at –80 °C for 4 h under Ar, distilled THF solution (20 mL) containing 0.5 equiv. of the 1,2-dibromoethane was added dropwise. After addition the oxidant, warming to ca. by leave to stand, the solution color changed

violet and the mixture was quenched with addition of H_2O (10 mL) dropwise. The organic solvent was evaporated, and the aqueous phase extracted by CH_2Cl_2 (50 mL × 3). The organic phase was dried by $MgSO_4$, and the solvent removed under vacuum. The crude product was purified by silica gel chromatography (100 % CH_2Cl_2 to 5 % CH_3OH/CH_2Cl_2 gradient elution), resulted in pale-yellow powder of dimphen ligand. ^{1}H-NMR (500 MHz, CD_2Cl_2): δ = 8.19 (d, 2H, H-C(4) or H-C(7)); 7.73 (s, 4H, H-C(5) or H-C(6)); 7.70 (d, 2H, H-C(3) or H-C(8)); 7.52 (d, 2H, H-C(3) or H-C(8)); 3.76 (s, 2 CH2); 2.91 (s, 2 Me) ppm.

Synthesis of complexes 1-4

Single crystals of complexes **1**–**4** were obtained using diffusion method with H-tube glassware under air. In the case of synthesis of **1**, **2** and **3**, the solution of MeOH (20 mL) containing respective metal ion (0.15 mmol; For **1**: $FeCl_2$, **2**: $CoCl_2$, **3**: $Mn(CH_3COO)_2{\cdot}4H_2O$), KSCN (0.30 mmol) and ascorbic acid was put on the one side of H tube and the solution of MeOH (20 mL) containing ligand (= dimphen) was added on the other side. Then MeOH solution was poured carefully not to mix each solution. Finally, the top of the H tube was covered with the parafilm in order to diffusion slowly. After 3-5 days, we could get the single crystal (**1**: orange needle, **2**: green needle, **3**: yellow block).
In the case of synthesis of **4**, the solution of MeOH (20 mL) dissolved $FeCl_2$ (0.15 mmol) and ascorbic acid was put on the one side of H tube and the solution of MeOH (20 mL) containing ligand (= dimphen) and 2 equiv. KSeCN was added on the other side. After doing the same method, we could get the red needle crystal.

Physical Measurements.

^{1}H-NMR spectra were measured on a JEOL (500-ECX) instrument operating at 500 MHz (using the deuterated solvents as the lock and tetramethylsilane as the internal reference). Magnetic susceptibilities of ground samples were measured on a superconducting quantum interference device (SQUID) magnetometer (Quantum Design MPMS-XL). Samples were put into a gelatin capsule, mounted inside a straw, and then fixed to the end of the sample transport rod. Single-crystal X-ray data for **1**, **3** and **4** were recorded on a Rigaku/MSC Saturn CCD diffractometer with confocal monochromated Mo Kα (λ = 0.7105 Å) and processed by using Rigaku/ CrystalClear software. Using Olex2, the structure was solved with the ShelXT structure solution program using Direct Methods and refined with the ShelXL refinement package using Least Squares minimization. The single crystal X-ray diffraction measurement for complex **2** was carried out on the MX1 beamline at the Australian Synchrotron. Diffraction data were collected using a Si<111> monochromated synchrotron X-ray radiation (λ = 0.71074) at 100(2) K with BlueIce software[3] and were corrected for Lorentz and polarization effects using the XDS software.[4] The structure was solved using SHELXT[5] and the full-matrix least-squares refinements were carried out using SHELXL-2014 via Olex2 interface.[6] All non-

hydrogen atoms were located from the electron density maps and refined anisotropically. Hydrogen atoms bound to carbon atoms were added in the ideal positions and refined using a riding model. The data completeness was a little low due to only one-circle data collection. In addition, part of the organic ligand was extensively disordered, and was modelled with equal occupancies. The Mössbauer spectra (isomer shift vs. metallic iron at room temperature) were recorded with a Wissel MVT-1000 Mössbauer spectrometer with a ^{57}Co/Rh source in the transmission mode.

Table S1. Elemental analysis data for (a) Fe1C30H22N6S2 :**1**, (b) Co1C30H22N6S2 :**2**, (c) Mn1C30H22N6S2 :**3** and (d) Fe1C30H22N6Se2 :**4**.

(a)			
	C	H	N
Found	61.40	3.76	14.30
Calcd.	61.44	3.78	14.33

(b)			
	C	H	N
Found	61.10	3.71	14.23
Calcd.	61.11	3.76	14.25

(c)			
	C	H	N
Found	61.51	3.74	14.33
Calcd.	61.53	3.79	14.35

(d)			
	C	H	N
Found	52.90	3.28	12.34
Calcd.	52.97	3.26	12.35

Table S2. Selected bond and other distances in **1**-**4**.

(Å)	**1**	**2**	**3**	**4**
M-N(1)	2.227(3)	2.195(8)*	2.306(4)	2.226(6)
M-N(2)	2.260(4)	2.22(2)*	2.295(4)	2.275(18)*
M-N(3)	2.091(4)	2.052(4)	2.265(4)	2.097(10)
M-N(4)	-	-	2.335(4)	-
M-N(5)	-	-	2.178(4)	-
M-N(6)	-	-	2.170(4)	-
M-M(*bc* plane)	8.709	8.595	8.802	8.687
M-M(*a* axis)	12.733	12.625	12.862	13.077
S-S(Se-Se)	3.340	3.307	3.360	3.359
π-π	3.963	3.631	3.8820	4.048

*disordered site

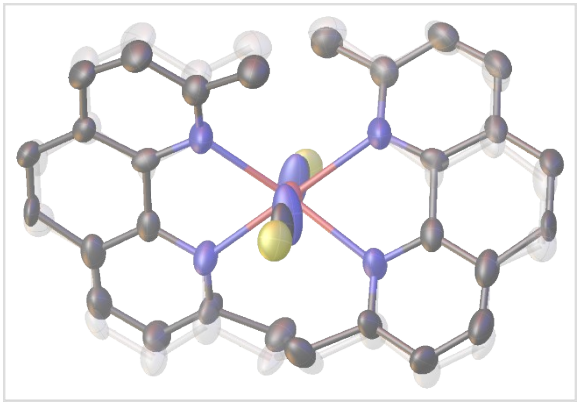

Figure S1. Thermal ellipsoid plot of **1** showing 50 % probability ellipsoids. Gray scaled molecule represents the disordered model. Color code: C, gray; N, blue; Fe, red; S, yellow. Hydrogen atoms were omitted for clarity.

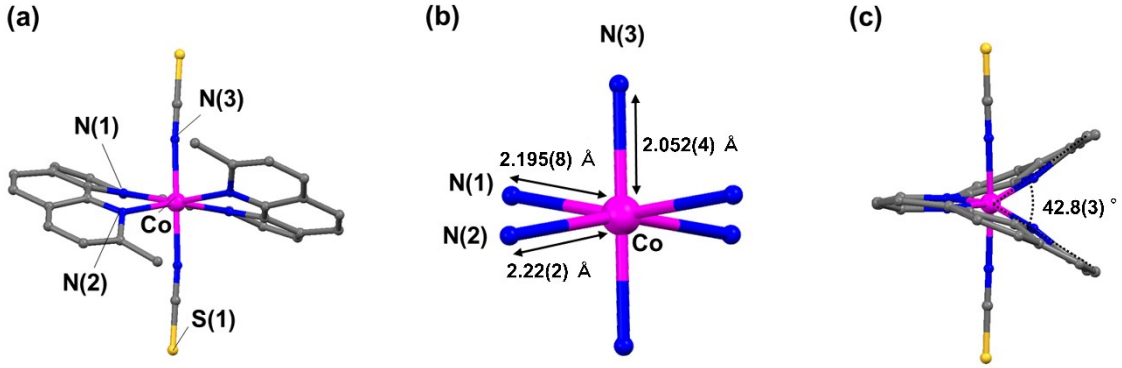

Figure S2. (a) Crystal structure of **2** at 100 K. Hydrogen atoms are omitted for clarity. Color code: C, gray; N, blue; Co, pink; S, yellow. (b) Bond lengths in the first coordination sphere. (c) Angle formed between the terminal methyl groups and the central metal.

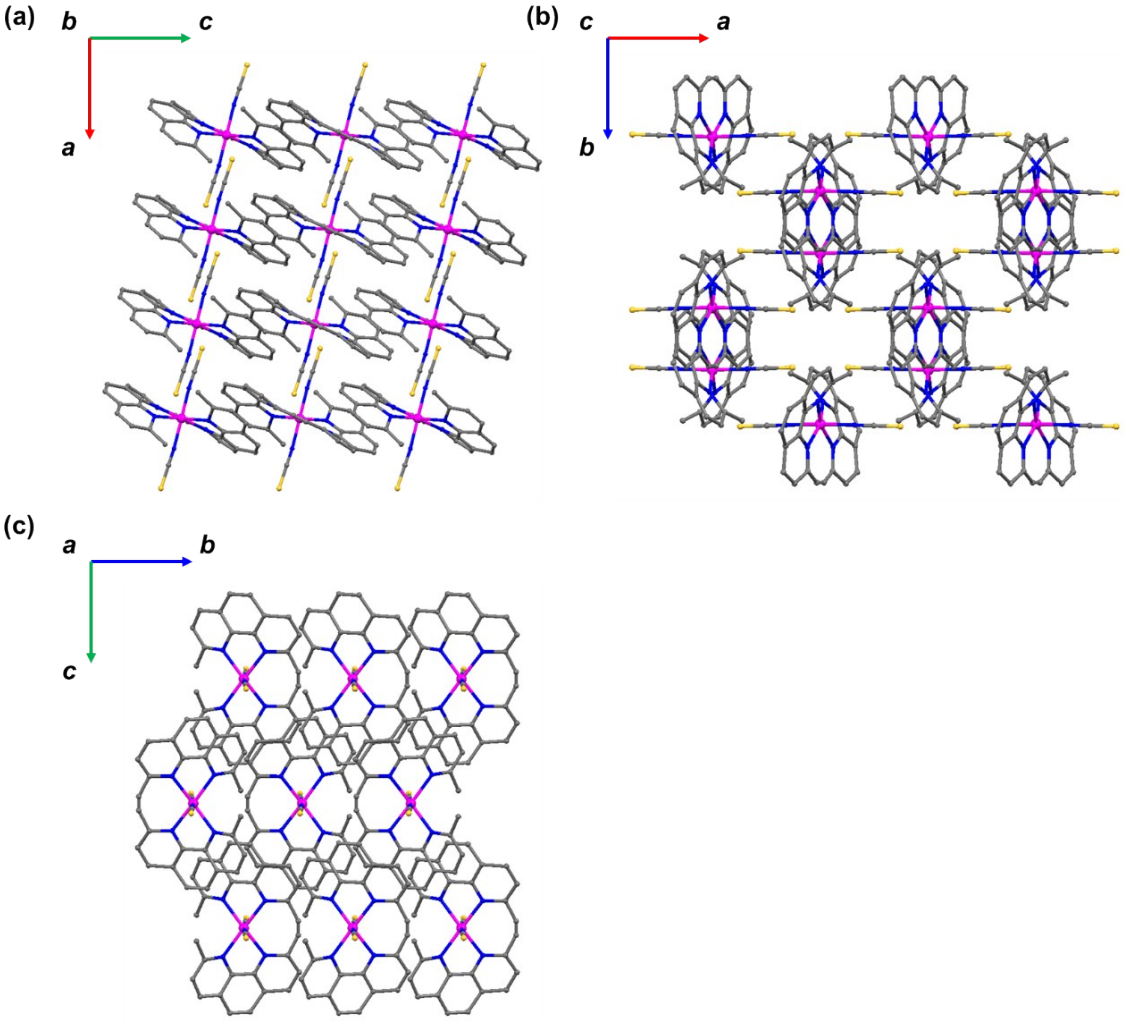

Figure S3. Crystal packing diagram for **2** at 100 K along the (a) *ac*, (b) *ab* and (c) *bc* plane.

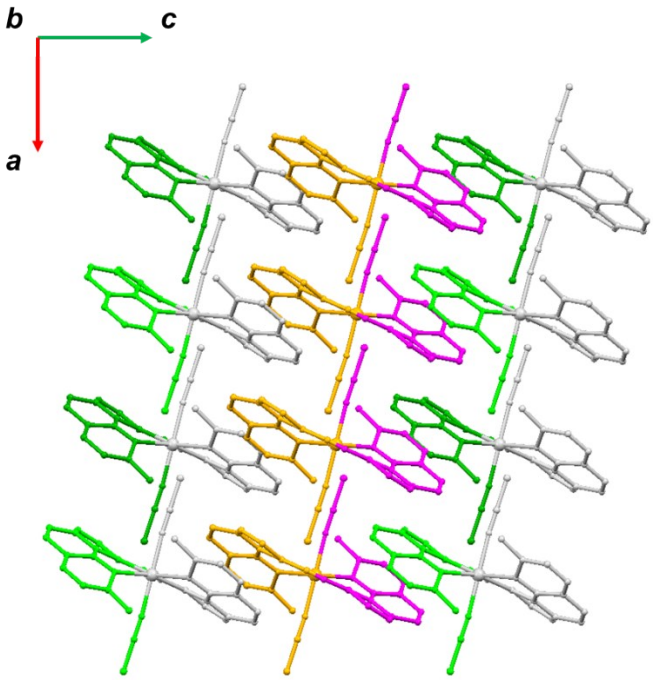

Figure S4. Symmetric operation for crystal packing of **2** in the *ac* plane. The molecules are colored by their symmetry relationship to the asymmetric unit.

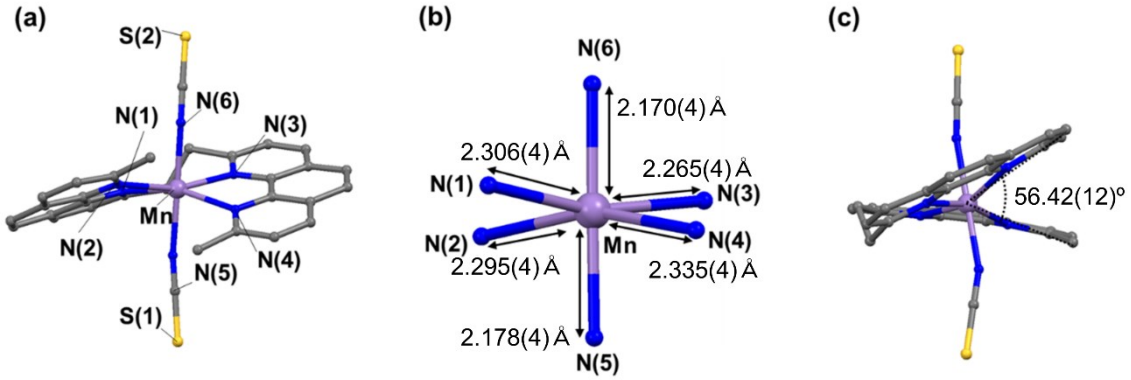

Figure S5. (a) Crystal structure of **3** at 100 K. Hydrogen atoms are omitted for clarity. Color code: C, gray; N, blue; Mn, purple; S, yellow. (b) Bond length in the first coordination sphere. (c) Angle formed between the terminal methyl groups and the central metal.

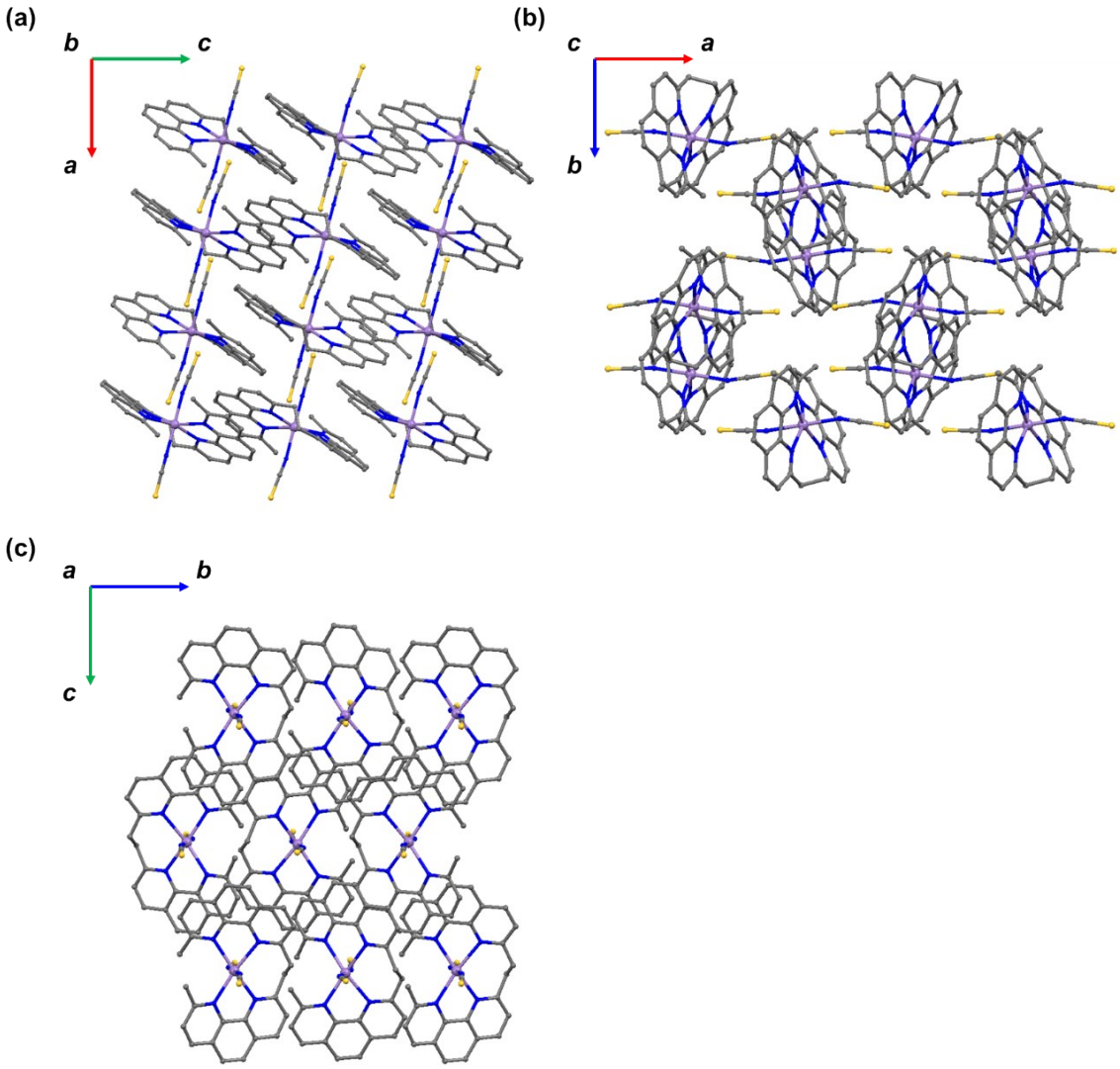

Figure S6. Crystal packing diagram for **3** at 100 K along the (a) *ac*, (b) *ab* and (c) *bc* planes.

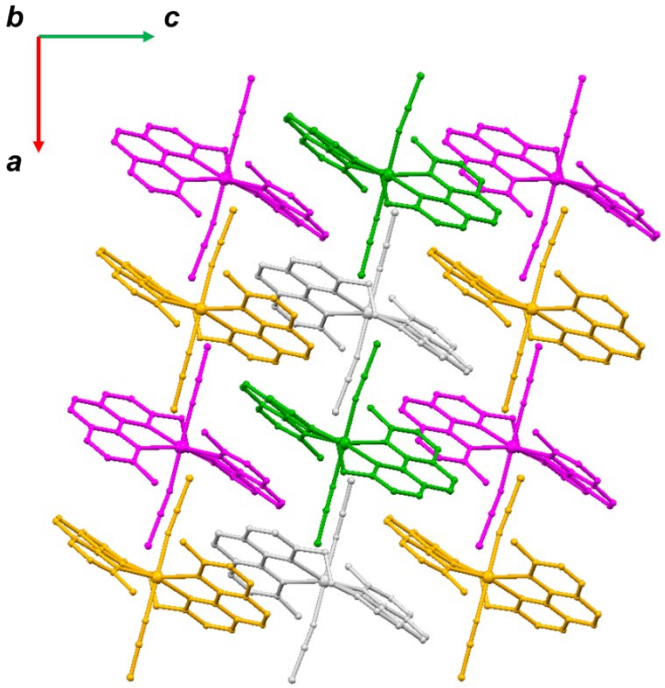

Figure S7. Symmetric operation for crystal packing of **3** in the *ac* plane. The molecules are colored by their symmetry relationship to the asymmetric unit.

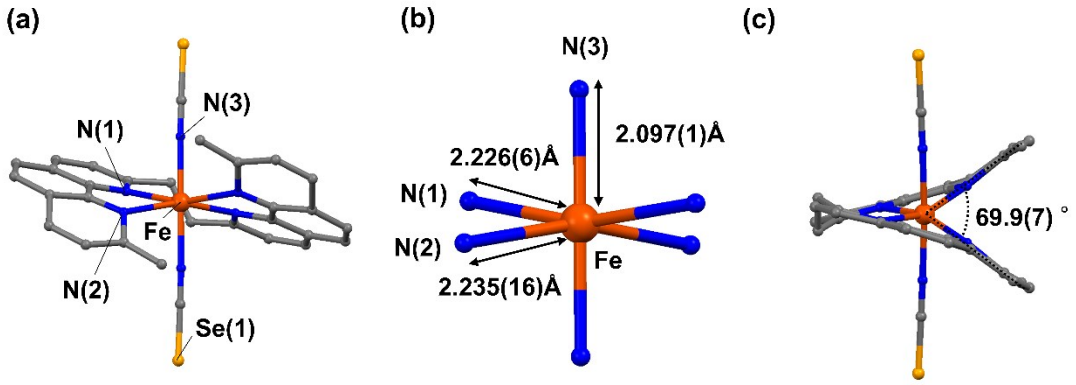

Figure S8. (a) Crystal structure of **4** at 100 K. Hydrogen atoms are omitted for clarity. Color code: C, gray; N, blue; Fe, orange; Se, yellow orange. (b) Bond lengths in the first coordination sphere. (c) Angle formed between the terminal methyl groups and the central metal.

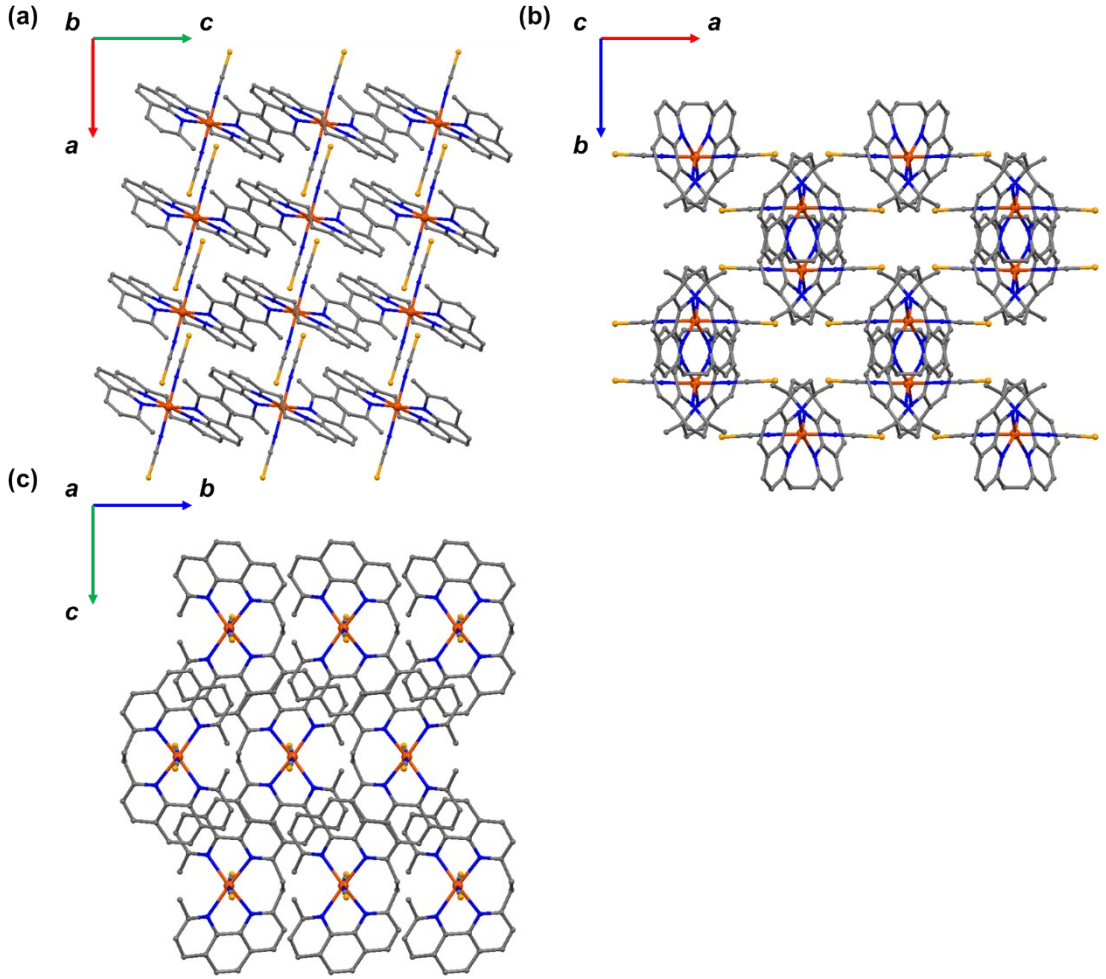

Figure S9. Crystal packing diagram for **4** at 100 K along the (a) *ac*, (b) *ab* and (c) *bc* planes.

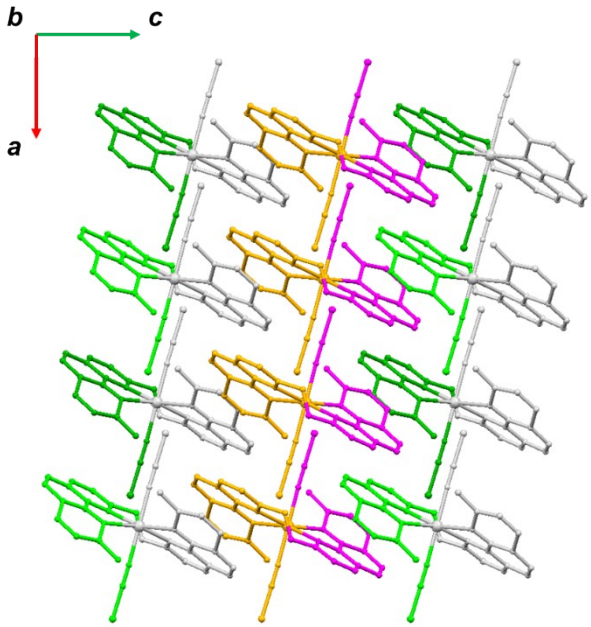

Figure S10. Symmetric operation of crystal packing of **4** in the *ac* plane. The molecules are colored by their symmetry relationship to the asymmetric unit.

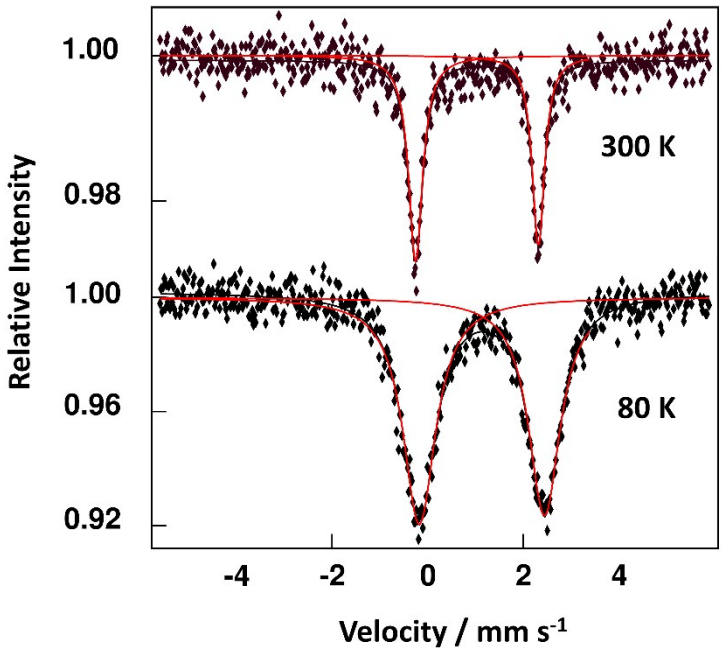

Figure S11. ^{57}Fe Mössbauer spectra of **1** at 300 K (top) and 80 K (bottom). The red solid lines are Lorentzian curves calculated using the parameters in text, which correspond to high-spin iron (II) ion species. [7]

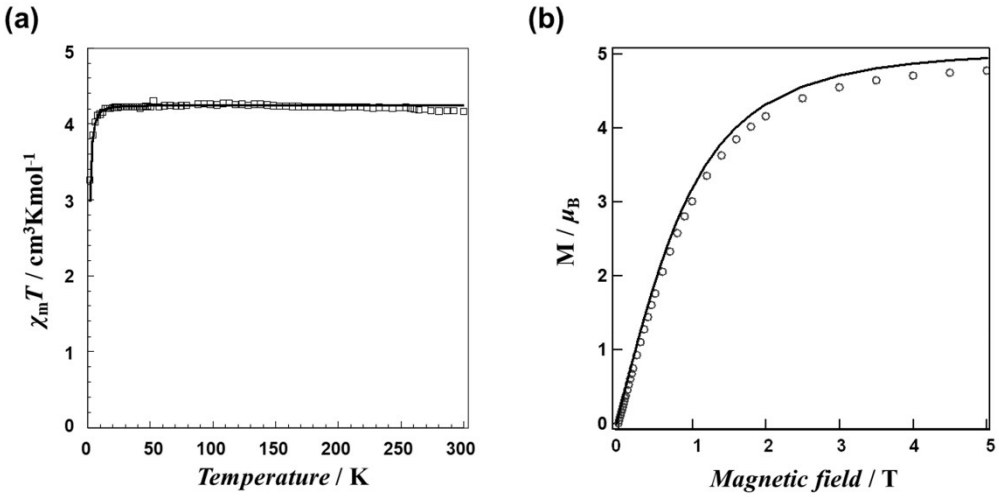

Figure S12. (a) Thermal variation of the $\chi_m T$ product per Mn(II) ion and (b) isothermal magnetization at 2 K for **3**. The solid line represents the Brillouin function for an $S = 5/2$ with $g = 2$.

Table S3. Axial and rhombic zero-field splitting parameters and *g* values for **2**.

Parameters	**2**
$\|D\|$ value (cm^{-1})	82.9
$\|E\|$ value (cm^{-1})	2.38
g_z value	2.48
$g_{x,y}$ value	2.43

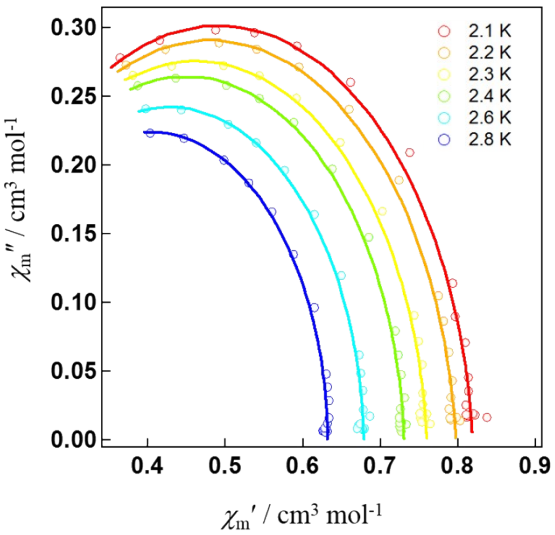

Figure S13. Cole-Cole plots of **2** taken at 1000 Oe dc field. The open circles represent the experimental data, and the solid lines represent the best fits of the experimental results with the generalized Debye model using Table S3.

Table S4. The fit parameters obtained from analyses of the ac susceptibilities of **2** under 1000 Oe dc field.

T / K	χ_s / cm^3 mol^{-1}	χ_t / cm^3 mol^{-1}	τ	α
2.1	$1.62(1)\times10^{-1}$	$8.19(1)\times10^{-1}$	$2.66(5)\times10^{-4}$	$5.51(6)\times10^{-2}$
2.2	$1.63(2)\times10^{-1}$	$7.97(3)\times10^{-1}$	$2.50(7)\times10^{-4}$	$5.52(8)\times10^{-2}$
2.3	$1.64(3)\times10^{-1}$	$7.60(0)\times10^{-1}$	$2.28(1)\times10^{-4}$	$4.90(7)\times10^{-2}$
2.4	$1.68(9)\times10^{-1}$	$7.30(6)\times10^{-1}$	$2.13(5)\times10^{-4}$	$3.82(0)\times10^{-2}$
2.6	$1.76(2)\times10^{-1}$	$6.78(8)\times10^{-1}$	$1.88(0)\times10^{-4}$	$2.34(4)\times10^{-2}$
2.8	$1.79(0)\times10^{-1}$	$6.32(0)\times10^{-1}$	$1.66(8)\times10^{-4}$	$7.87(4)\times10^{-3}$

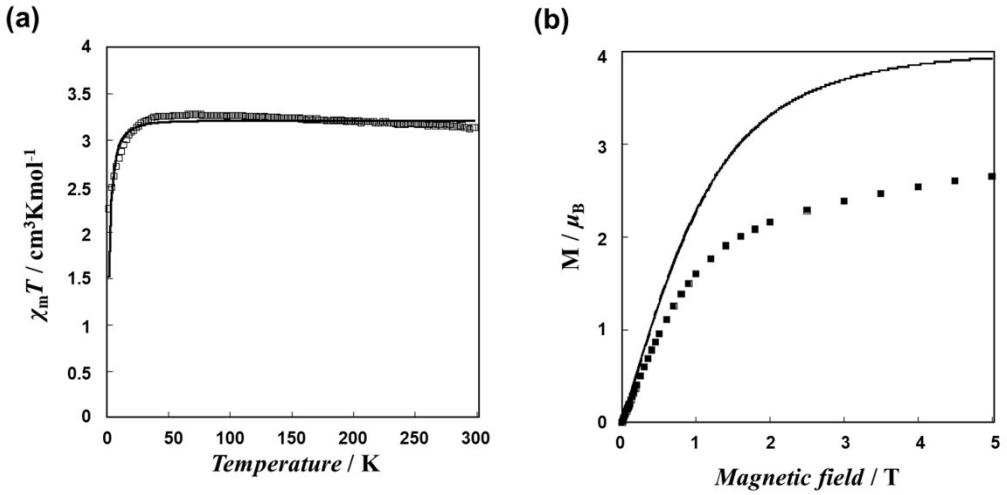

Figure S14. (a) Thermal variation of the $\chi_m T$ product per Fe(II) ion and (b) isothermal magnetization at 2 K for **4**. The solid line represents the Brillouin function for an $S = 2$ ion with $g = 2$.

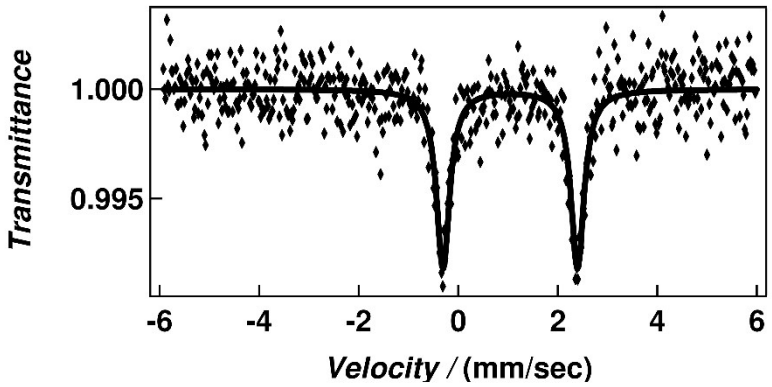

Figure S15. ^{57}Fe Mössbauer spectra of **4** at 300 K. The solid line is Lorentzian curves calculated using the parameters (QS = 2.70 cm^{-1}, IS = 1.04 cm^{-1}), which corresponds to high-spin iron (II) ion unit. [7]

REFERENCES

[1] J.-M. Lehn and R. Ziessel, *Helv. Chim. Acta*., 1988, **71**, 1511.

[2] M.-T. Youinou, R. Ziessel, and J.-M. Lehn, *Inorg. Chem*., 1991, **30**, 2144.

[3] T. M. McPhillips, S. E. McPhillips, H. J. Chiu, A. E. Cohen, A. M. Deacon, P. J. Ellis, E. Garman, A. Gonzalez, N. K. Sauter, R. P. Phizackerley, S. M. Soltis, P. Kuhn, J. Synchrotron Rad. 2002, 9, 401.

[4] W. Kabsch, J. *Appl. Crystallogr.* 1993, 26, 795.

[5] (a) G. M. Sheldrick, *Acta Crystallogr., Sect. A*. 2015, 71, 3; (b) SHELXT-2014, G. M. Sheldrick, University of Göttingen, 2014.

[6] O. V. Dolomanov, L. J. Bourhis, R. J. Gildea, J. A. K. Howard, H. Puschmann, *J. Appl. Crystallogr.* 2009, **42**, 339.

[7] D. C. Figg, R. H. Herber, J. A. Potenza, *Inorg. Chem*., 1992, **31**, 2111-2117.